RESEARCH ARTICLE

Macromolecular Chemistry and Physics
www.mcp-journal.de

Design and Construction of Furan-Based and Thiophene-Based Salicyladazine Bisbenzoxazine Resins with High Thermal Stability and Tunable Surface Properties

Yang-Chin Kao, Mohamed Gamal Mohamed, Chia-Husan Chiang, and Shiao-Wei Kuo**

Two disubstituted bisbenzoxazine (Bz) monomers are synthesized using furan (Fa) and thiophene (Th) derivatives: bis((3-(furan-2-ylmethyl)-7-ol-3,4-dihydro-2H-benzo[e][1,3] oxazin-6-yl)methylene)hydrazine (BAZ-Fa-BZ) and bis((3-(thiophen-2-ylmethyl)-7-ol-3,4-dihydro-2H-benzo[e][1,3] oxazin-6-yl)methylene)hydrazine (BAZ-Th-BZ). These monomers are synthesized via Mannich condensation of salicylaldazine (1,2-bis(2,4-dihydroxybenzylidene) hydrazine (BAZ—4OH)) and paraformaldehyde $(CH_2O)_n$, with furfurylamine ($FacNH_2$) and thiophene-2-methenamine ($Th—NH_2$), respectively. The chemical structures of BAZ-Fa-BZ and BAZ-Th-BZ are affirmed using Fourier-transform infrared spectroscopy (FTIR) and NMR, respectively. A thorough investigation of the thermal polymerization process of BAZ-Fa-BZ and BAZ-Th-BZ is conducted using differential scanning calorimetry (DSC), thermogravimetric analysis (TGA), and in situ FTIR spectra (ranging from 25 to 250 °C). Poly(BAZ-Fa-BZ) exhibits superior thermal properties with a thermal decomposition temperature (T_{d10}) of 402 °C and a char yield of 58 wt% after thermal treatment at 250 °C, along with a lower surface free energy of 28.9 mJ m^{-2} compared to poly(BAZ-Th-BZ) (T_{d10} = 359 °C, char yield = 48 wt%, and surface free energy = 34.1 mJ m^{-2}). Additionally, poly(BAZ-Th-BZ/BAZ-Fa-BZ) blend with a ratio of 1/3 after thermal curing at 250 °C demonstrates the highest T_{d10} of 395 °C and a char yield of 60 wt%. Photoluminescence (PL) measurements conducted in the solid state reveal that BAZ-Th-BZ, BAZ-Fa-BZ, and their blends emit green light when excited at a wavelength of 365 nm.

1. Introduction

In recent years, benzoxazines (BZ) have attracted considerable attention as thermosetting resins due to their remarkable properties: low surface free energy, excellent thermal and dimensional stability, remarkable flame retardancy, versatile molecular design, and exceptional electrical resistance.[1–10] These derivatives, containing six-membered heterocyclic rings, can be synthesized using the Mannich condensation method, requiring formaldehyde, a primary aromatic or aliphatic amine, and a phenolic derivative.[11–20] The physical properties of polybenzoxazines (PBZs) could be tailored through various methods, such as the introduction of allyl, bromophenyl, hydroxyl, nitrile, or phenyl groups, or by incorporating strong hydrogen bonding moieties into the benzoxazine monomers.[1,13,21–23] These modifications lead to materials with diverse thermal and mechanical properties, as well as enhanced resistance to solvents.[13] For example, the hydrophobic surface characteristics of PBZs are greatly influenced by the degree of intramolecular hydrogen bonding between the nitrogen atoms in the Mannich bridge and the phenolic OH groups, occurring post the thermal ring-opening polymerization (ROP) of BZ monomers.[24,25]

The luminescent properties of many fluorescent materials tend to diminish when they aggregate in a suboptimal solvent or a solid state.[26–32] This phenomenon, known as aggregation-caused quenching (ACQ), imposes significant limitations on the potential applications of these materials, particularly in fields like organic light-emitting materials or fluorescent chemosensing.[26–32] However, Tang and co-workers have reported that numerous materials exhibit light emission when dispersed in a poor solvent or when formed into a film in a nanoaggregate state.[33–35] These fascinating phenomena are termed aggregation-induced emission (AIE). AIE is caused by various processes, such as planarity and rotation ability, twisting intramolecular charge transfer (TICT), and restricted intramolecular rotation (RIR).[36–38] Although the mechanical and thermal properties of BZ have been extensively researched, there has been comparatively less investigation into luminous

Y.-C. Kao, M. G. Mohamed, C.-H. Chiang, S.-W. Kuo
Department of Materials and Optoelectronic Science
Center of Crystal Research
National Sun Yat-Sen University
Kaohsiung 804, Taiwan
E-mail: mgamal.eldin12@aun.edu.eg; kuosw@faculty.nsysu.edu.tw
M. G. Mohamed
Chemistry Department
Faculty of Science
Assiut University
Assiut 71515, Egypt
S.-W. Kuo
Department of Medicinal and Applied Chemistry
Kaohsiung Medical University
Kaohsiung 807, Taiwan

The ORCID identification number(s) for the author(s) of this article can be found under https://doi.org/10.1002/macp.202400091

DOI: 10.1002/macp.202400091

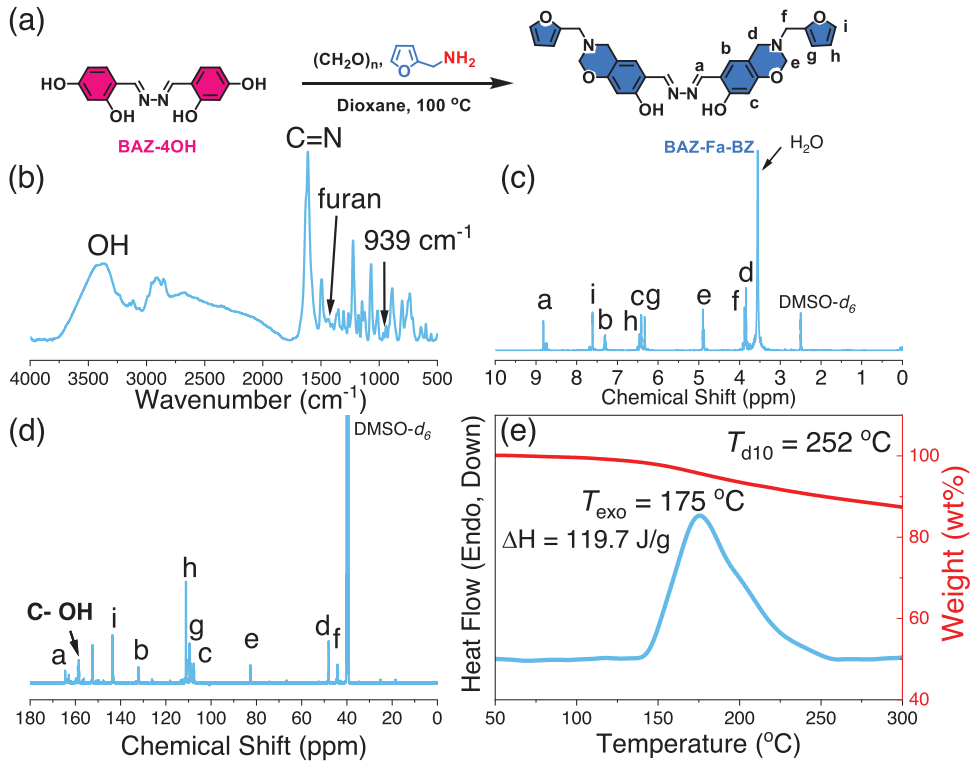

Figure 1. a) The synthesis of BAZ-Fa-BZ monomer and its corresponding b) FTIR, c) ^{1}H NMR (recorded in dimethylsulfoxide-d_6 (DMSO-d_6), d) ^{13}C NMR spectra (recorded in dimethylsulfoxide-d_6 DMSO-d_6), and e) TGA and DSC analyses of BAZ-Fa-BZ.

benzoxazines.[39,40] For example, the Hui group demonstrated that picric acid (PA) could be detected using a tetraphenylethene decorated polybenzoxazines (TPE–BOZ) precursor as a probe.[41] Additionally, Shi et al. reported that TPE-decorated PBZ exhibits an AIE property and serves as a fluorescent probe for 2,4-dinitrophenol (DNP), with a detection limit of ≈7.4×10^{-7} M.[42]

Due to its furan (Fa) ring capable of crosslinking, furfurylamine (Fa—NH_2) is commonly employed as a modifier in high-performance thermosetting materials. Incorporating Fa groups into benzoxazine enhances the polymer's crosslinking density, thereby boosting its heat stability and T_g by the creation of Mannich bridges between furfurylamine during polymerization.[43–49] Because of its abundant π-electrons and high reactivity, thiophene (Th), a sulfur-containing heterocyclic molecule, readily contributes to the formation of polymer networks in materials. According to Mukherjee and Lochab,[50] the Th unit facilitates the formation of highly cross-linked networks in PBZ, offering more reactive sites. Additionally, the early thermal stability and high char yield values of Th-containing PBZ indicate their inherent self-extinguishing properties due to the inclusion of both N and S atoms in the networks.[51–53] Based on the above information, in this study, we utilized bisbenzoxazine monomers featuring intramolecular hydrogen bonding within the salicylaldazine structure to synthesize bis((3-(furan-2-ylmethyl)-7-ol-3,4-dihydro-2H-benzo[e][1,3] oxazin-6-yl)methylene)hydrazine (BAZ-Fa-BZ) and bis((3-(thiophen-2-ylmethyl)-7-ol-3,4-dihydro-2H-benzo[e][1,3] oxazin-6-yl)methylene)hydrazine (BAZ-Th-BZ) using paraformaldehyde $(CH_2O)_n$ Fa—NH_2, and naturally renewable amine derivatives, as well as thiophene-2-methenamine (Th—NH_2) commonly found in petroleum, coal tar, and shale oil. The synthesis process involved Mannich condensation of difunctionalized benzoxazine resins derived from both bio-based and petrochemical sources (BAZ-Fa-BZ and BAZ-Th-BZ). After ROP at 250 °C, TGA data revealed that in comparison to poly(BAZ-Th-BZ) with a T_{d10} of 359 °C and a char yield of 48 wt% and a surface free energy of 34.1 mJ m^{-2}, poly(BAZ-Fa-BZ) exhibited superior thermal properties, boasting a T_{d10} of 402 °C and a char yield of 58 wt%. Moreover, the blend with a ratio of 1/3, poly(BAZ-Th-BZ/BAZ-Fa-BZ), displayed the highest T_{d10} of 395 °C and achieved the maximum char production of 60 wt%.

2. Results and Discussion

2.1. Synthesis and Characterization of BAZ-Fa-BZ

The synthetic pathway of the BAZ-Fa-BZ monomer via a straightforward Mannich condensation reaction involving salicylaldazine (1,2-bis(2,4-dihydroxybenzylidene)hydrazine (BAZ—4OH)), $(CH_2O)_n$, and Fa—NH_2 is depicted in **Figure 1a**. The chemical structure and attributes of the newly synthesized BAZ-Fa-BZ were validated through various analyses including Fourier-transform infrared spectroscopy (FTIR), ^{1}H NMR, ^{13}C NMR, TGA, and DSC, as delineated in Figure 1b–e. In the FTcIR analyses, the broad absorption bands observed at 3379 cm^{-1} were attributed to O—H stretching, while peaks at 3147, 3115, and 3062 cm^{-1}, indicated sp^2-hybridized C—H stretching. The presence of the salicylaldazine structure was evidenced by

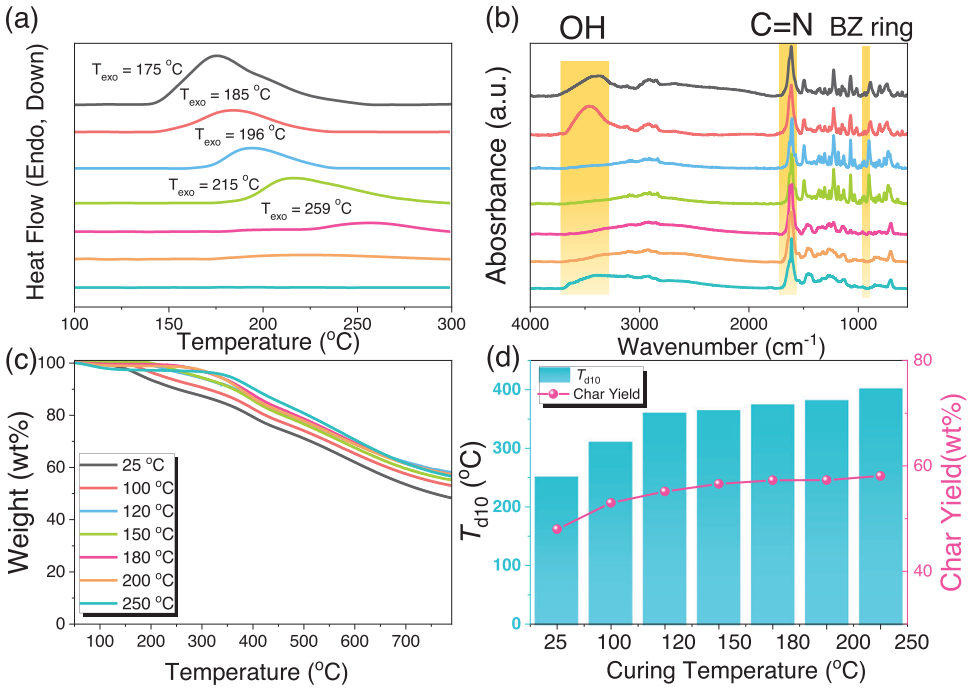

Figure 2. a) DSC, b) FTIR spectra, c) TGA analyses, and d) T_{d10} and char yield values of BAZ-Fa-BZ monomer before and after thermal curing polymerization at different temperatures (25–250 °C).

signals of C═N at 1630 cm^{-1}. Following the Mannich condensation reaction, distinct absorption peaks at 1441 and 737 cm^{-1} emerged, indicative of the furan structure.[54,55]

Additionally, absorption peaks associated with the oxazine ring emerged at 1364 and 939 cm^{-1}. The oxazine ring's C—O—C group exhibited an asymmetric stretching vibration at 1225 cm^{-1}, as depicted in Figure 1b. Figure 1c demonstrates the confirmation of the oxazine ring formation in BAZ-Fa-BZ, with distinct peaks observed at 4.90 ppm (e) and 3.84 ppm (d), corresponding to the O—$\underline{CH_2}$—N and Ar—$\underline{CH_2}$—N units, respectively. Furthermore, peaks at 8.81, 6.41–7.29, and 3.87 ppm were assigned to the protons of N═C—H, aromatic C—H, and Fa—CH_2—N units, respectively. Additionally, protons of the Fa units were observed at 6.33, 6.45, and 7.60 ppm (g, h, I). In Figure 1d, the ^{13}C NMR spectrum of BAZ-Fa-BZ displayed signals ranging from 107 to 158 ppm, corresponding to the carbon nuclei of the aromatic and Fa rings (g, h, i). Furthermore, BAZ-Fa-BZ exhibited characteristic signals at 48, 82, and 164 ppm, representing the carbon nuclei of Ar—CH_2N, O—CH_2N, and azine (CH═N—N═CH) units, respectively. A peak at 44 ppm evidenced the carbon nuclei of Fa—$\underline{CH_2}$—N. Moreover, DSC and TGA analyses of the uncured BAZ-Fa-BZ monomer revealed an ROP reaction occurring at 175 °C, with a thermal decomposition temperature (T_{d10}) of 252 °C, as indicated in Figure 1e. **Figure** 2a,b presents the DSC analyses and FTIR spectra, respectively, of BAZ-Fa-BZ at various stages of thermal treatment. With an increase in thermal treatment temperature from 100 to 180 °C, the thermal curing peaks of BZ shifted toward higher values. Subsequent thermal treatment from 200 to 250 °C led to the complete disappearance of thermal ROP peaks, suggesting the formation of a highly crosslinked network 3D structure of PBZ with additional crosslinking structure from the Fa moiety,[56,57] as depicted in Figure 2a. Concurrently, Figure 2b illustrates that the absorption bands of the BZ ring at 1364 and 939 cm^{-1} decreased with increasing curing temperature from 100 to 180 °C, and these bands completely disappeared after 200 and 250 °C, aligning with the findings from the DSC analyses shown in Figure 2a. In Figure 2c, TGA analyses revealed that the untreated BAZ-Fa-BZ monomer exhibited a T_{d10} of 252 °C and a char yield of 48 wt%. Upon thermal treatment, the T_{d10} values were observed to be 311, 361, 365, 375, 382, and 402 °C successively, and the corresponding char yields were 53, 55, 56, 57, 57, and 58 wt%, as evident in Figure 2c,d.

Figure S4 (Supporting Information) displays the possible polymerization mechanism of BAZ-Fa-BZ at high temperatures. This indicates that intramolecular OH—N hydrogen bonding improved the T_{d10}, and the increased char yield was associated with the formation of a cross-linked network structure involving both the BZ ring and furan ring. **Figure** 3a–c presents a summary of the water contact angle (WCA), di-iodomethane contact angle (DIMCA), and surface free energy for uncured and cured BAZ-Fa-BZ. The WCAs of BAZ-Fa-BZ were measured as 98.5°, 100.7°, 103.4°, 106.6°, 109.8°, 113.5°, and 113.8° sequentially, while the DIMCAs of BAZ-Fa-BZ were recorded as 49.5°, 52.4°, 60.1°, 60.5°, 64.1°, 64.9°, and 59.7°, respectively. Surface free energy values for BAZ-Fa-BZ were documented as 34.8, 33.1, 28.7, 28.3, 26.2, 25.8, and 28.9 mJ m^{-2}. Among these, the WCA values of BAZ-Fa-BZ increased after thermal treatment, correlating with the ring-opening reaction of the oxazine unit in BAZ-Fa-BZ. This suggests an increase in OH—N and OH—π hydrogen bonding within the molecules, originating from Mannich bridges, along with additional OH—N hydrogen bonding within molecules between the azine units, as illustrated in Figure 3d.[58–61]

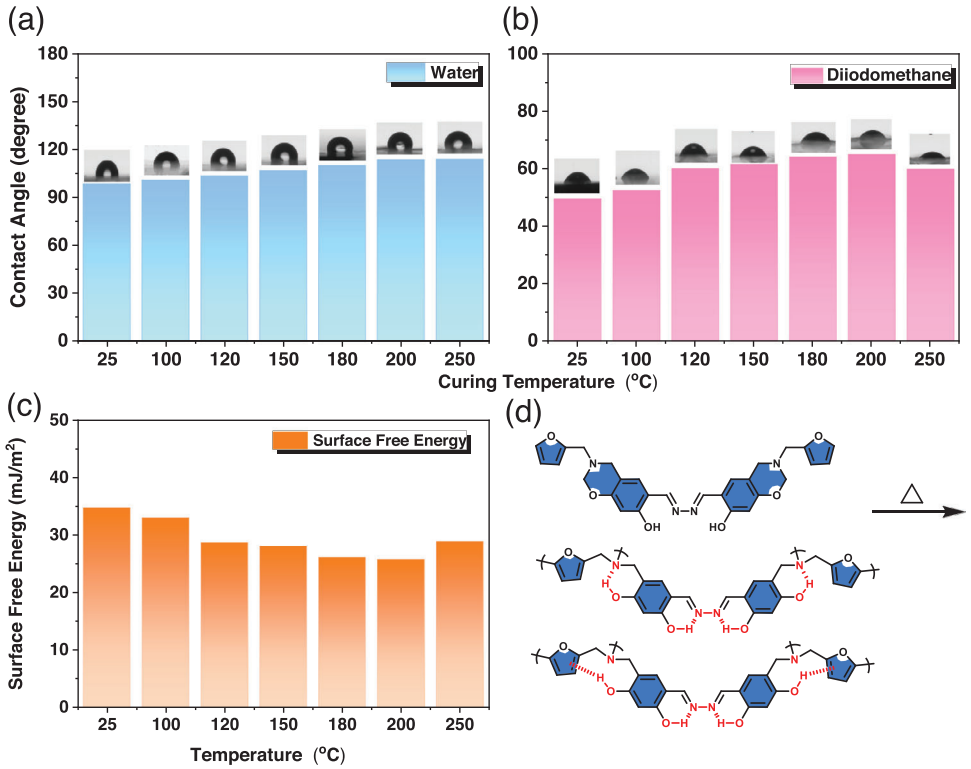

Figure 3. a) Water (H_2O) and b) di-iodomethane (CH_2I_2) contact angles, c) their corresponding surface free energy of BAZ-Fa-BZ before and after thermal curing polymerization at different temperatures (25– 250 °C), and d) the intramolecular hydrogen bonding after thermal ROP of BAZ-Fa-BZ.

2.2. Synthesis and Characterization of BAZ-Th-BZ

Figure 4a illustrates the synthetic pathway leading to the BAZ-Th-BZ monomers from BAZ—4OH, Th—NH_2, and $(CH_2O)_n$ via the Mannich condensation reaction. The chemical structure and characteristics of BAZ-Th-BZ were confirmed through analysis using FTIR, NMR, and DSC, as shown in Figure 4b–e. In the FTIR analyses, the broad absorption bands observed at 3418 cm^{-1} were assigned to O—H stretching, while peaks at 3067 cm^{-1} indicated sp^2-hybridized C—H stretching. After the Mannich condensation reaction, distinct absorption peaks at 1444 and 710 cm^{-1} indicated the presence of the Th ring in the BAZ-Th-BZ structure.[62,63] Additionally, absorption peaks corresponding to the BZ ring at 1359 and 947 cm^{-1} were evident. Furthermore, a peak at 1225 cm^{-1}, attributed to the Ar—CH_2—N linkage between the Th and BZ groups, is observed in Figure 4b. In Figure 4c, the confirmation of oxazine ring formation in BAZ-Th-BZ was established by distinct peaks at 4.95 ppm (e) and 4.05 ppm (d), corresponding to Ar—$\underline{CH_2}$—N and O—$\underline{CH_2}$—N units, respectively. Additionally, the BAZ-Th-BZ monomer exhibited peaks at 8.81 and 3.90 ppm, signifying the protons of N=C—H, and Th—CH_2—N units, respectively. Moreover, protons of the Th unit in the BAZ-Th-BZ were identified at 6.98, 7.32, and 7.48 ppm (g, i, h). In Figure 4d, the ^{13}C NMR spectrum of BAZ-Th-BZ revealed signals within the range of 107–158 ppm, indicating the presence of carbon nuclei associated with the aromatic and Th rings (g, h, i). Additionally, distinct signals at 50, 82, and 164 ppm were evident in BAZ-Th-BZ, denoting the carbon nuclei linked to Ar—CH_2—N, O—CH_2—N units, and azine units, respectively. The peak indicated the carbon nuclei of the Th—CH_2—N unit at 43 ppm. Furthermore, TGA and DSC analyses of the uncured BAZ-Th-BZ showed a melting point (T_m) at 197 °C, a curing peak at 214 °C, and a T_{d10} of 271 °C. We conducted both DSC analyses and FTIR spectra recordings of BAZ-Th-BZ at various stages of thermal treatment (**Figure** 5a,b). As the thermal treatment temperature increased from 100 to 180 °C, the melting point decreased from 197 to 184 °C, and the curing peaks shifted from 214 to 211 °C. Around 200 °C, the melting point disappeared, and the curing peaks shifted to 234 °C, indicating the involvement of the Th ring in the polymerization events. The curing peaks completely vanished at 250 °C, as shown in Figure 5a. These observations are in line with the findings from the FTIR spectra in Figure 5b. With the increasing curing temperature from 100 to 180 °C, the absorption bands associated with the oxazine unit, peaking at 1359 and 947 cm^{-1}, decreased in intensity and eventually disappeared entirely at 200 °C. In Figure 5c, TGA analyses unveiled that the untreated BAZ-Th-BZ monomer exhibited a T_{d10} of 263 °C and a char yield of 50.5 wt%. Following heat treatment, the T_{d10} values ascended to 283, 285, 286, 292, 316, and 365 °C successively, accompanied by corresponding char yields of 51.24, 51.36, 51.37, 51.63, 51.83, and 52.8 wt%, as depicted in Figure 5c,d. Figure S5 (Supporting Information) shows the possible polymerization mechanism of BAZ-Th-BZ at high temperatures.

The WCA, DIMCA, and surface free energy for uncured and cured BAZ-Th-BZ are presented in **Figure** 6a–c. The corresponding values of WCAs and DIMCAs of BAZ-Th-BZ were 78.6°, 80.9°, 85°, 80.9°, 83.7°, 89.3°, and 79.8°, and 25.6°, 44.4°, 54.2°, 55°, 57.4°, 62.1°, and 61.9° successively. The values of surface

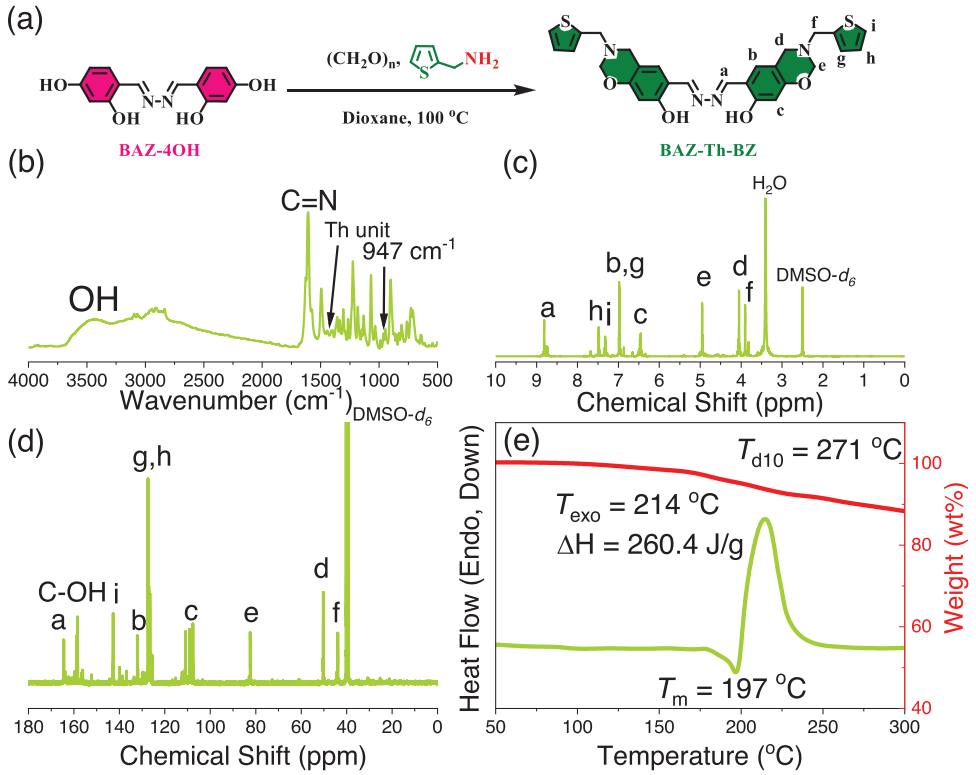

Figure 4. a) The synthesis of BAZ-Th-BZ and the corresponding b) FTIR, c) ^{1}H NMR (recorded in DMSO-d_6), d) ^{13}C NMR (recorded in DMSO-d_6), and e) TGA and DSC profiles of BAZ-Th-BZ.

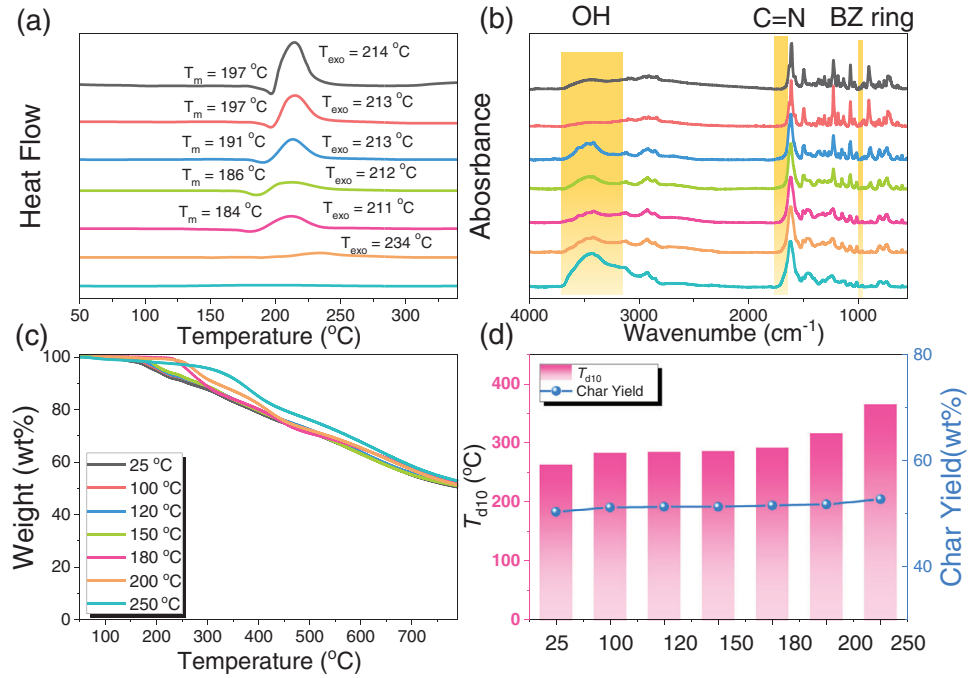

Figure 5. a) DSC, b) FTIR, c) TGA analyses, and d) summarized T_{d10} values and char yields of BAZ-Th-BZ.

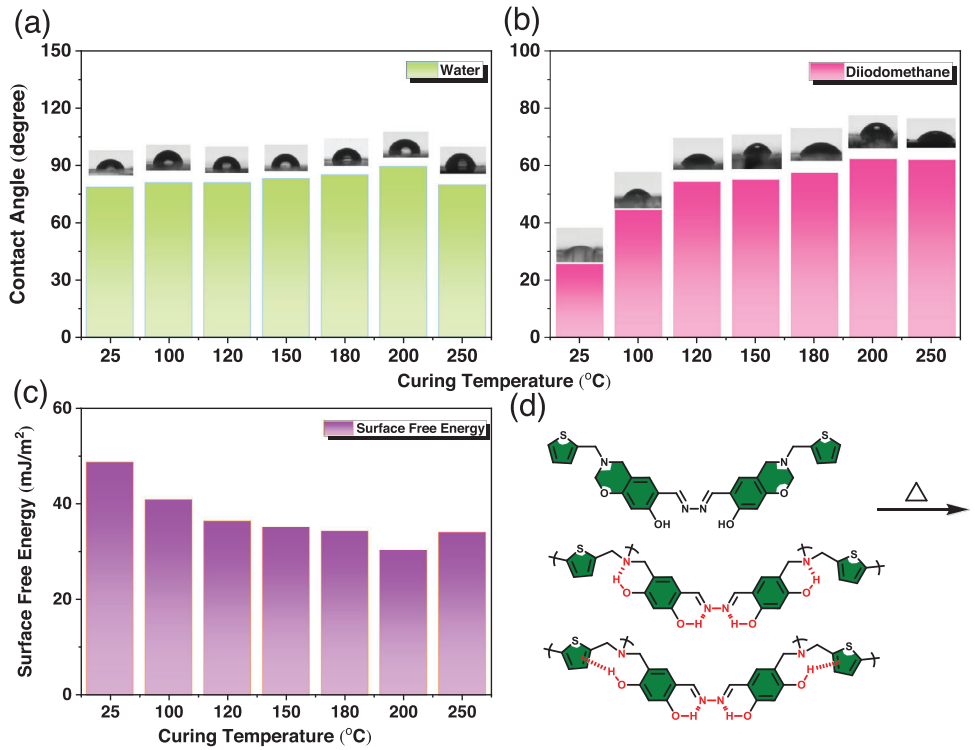

Figure 6. a) Water contact angle, b) di-iodomethane contact angle, c) surface free energy of BAZ-Th-BZ before and after thermal curing polymerization at different temperatures (25–250 °C), and d) the hydrogen bonding for the ring-opening polymerization of BAZ-Th-BZ.

free energy of BAZ-Th-BZ were 48.7, 40.9, 35.3, 36.4, 34.3, 30.39, and 34.1 mJ m^{-2}. The DIMCA values of BAZ-Th-BZ showed better lipophilicity before thermal treatment because the polarity of the Th group was lower than that of the Fa group. Based on the thermal treatment (100–250 °C), DIMCA values of BAZ-Th-BZ increased and lipophilicity decreased, which was under the ring-opening reaction of BAZ-Th-BZ, indicating the formation of hydrogen bonding and resulting in enhanced polarity, as demonstrated in Figure 6d.

2.3. Thermal Polymerization of BAZ-Th-BZ/BAZ-Fa-BZ Blends

In **Figure** 7a, the FTIR spectra of the BAZ-Th-BZ/BAZ-Fa-BZ blends reveal broad absorption bands ranging from 3677 to 3033 cm^{-1}, corresponding to O—H stretching, and a signal of C═N stretching at around 1609 cm^{-1}. BZ absorption peaks in the BAZ-Th-BZ/BAZ-Fa-BZ blends are observed at 1356 and 945 cm^{-1}. As the ratio of BAZ-Fa-BZ monomer increases, the curing peaks shift to lower temperatures, from 214 to 175 °C, as shown in Figure 7b,c, which displays the TGA analyses of BAZ-Th-BZ, BAZ-Fa-BZ, and BAZ-Th-BZ/BAZ-Fa-BZ after blending. Among these blends, BAZ-Th-BZ/BAZ-Fa-BZ = 3/1 exhibits the lowest char yield at 47 wt% and T_{d10} = 268 °C. Conversely, BAZ-Th-BZ/BAZ-Fa-BZ = 1/1 demonstrates the highest char yield at 49 wt% and T_{d10} = 269 °C. BAZ-Th-BZ/BAZ-Fa-BZ = 1/3 indicates that the values of char yield and T_{d10} are 47 wt% and 301 °C, respectively. Moreover, Figure 7d summarizes the char yield and T_{d10} values of BAZ-Th-BZ, BAZ-Fa-BZ, and BAZ-Th-BZ/BAZ-Fa-BZ blends.

In **Figure** 8a, the FTIR spectra of BAZ-Th-BZ/BAZ-Fa-BZ = 3/1 blend under different thermal curing treatments reveal broad O—H stretching from 3675 to 3027 cm^{-1}, and the signal of C═N stretching shifts from 1610 to 1614 cm^{-1}. The peak corresponding to the BZ ring in the BAZ-Th-BZ/BAZ-Fa-BZ decreases from 25 to 180 °C and disappears after 200 °C. Figure 8b–d depicts dynamic DSC analyses of BAZ-Th-BZ/BAZ-Fa-BZ after thermal treatments.

BAZ-Th-BZ/BAZ-Fa-BZ = 3/1 hybrids show an increase in curing temperature from 25 to 200 °C, with a complete disappearance of the curing peak observed at 250 °C in Figure 8b. BAZ-Th-BZ/BAZ-Fa-BZ = 1/1 hybrids exhibit a similar trend, with the curing peak disappearing at 250 °C after increasing from 25 to 200 °C, as shown in Figure 8c. BAZ-Th-BZ/BAZ-Fa-BZ = 1/3 hybrids indicate a shift in the curing peak from 187 to 303 °C, as depicted in Figure 8d. Among these materials, an increase in the BAZ-Fa-BZ ratio tends to raise the thermal polymerization temperature of the BAZ-Th-BZ/BAZ-Fa-BZ blend. This signifies that the hydrogen bonding force influences the BZ ring. As the proportion of hydrogen bonds in the molecule increases, the BZ ring-opening temperature is elevated for the ring-opening process. However, the increase is not greater than that of pure BAZ-Fa-BZ because the Th group reduces the cross-linking between the BZ groups. In other words, as the BAZ-Th-BZ content increases, the curing temperature also increases. **Figure** 9 presents TGA analyses conducted on various BAZ-Th-BZ/BAZ-Fa-BZ blends. The results indicate an improvement in the T_{d10} values following thermal treatment due to the formation of hydrogen bonds within the BZ resin. As temperatures increase, the

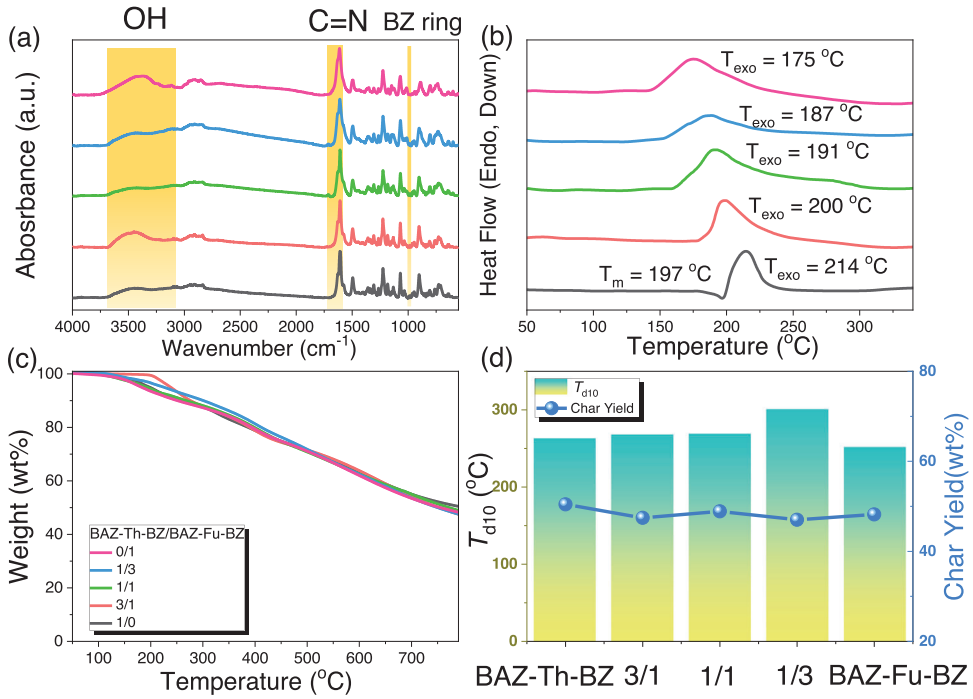

Figure 7. a) FTIR, b) DSC, c) TGA analyses, and d) summarized T_{d10} values and char yields of BAZ-Th-BZ/BAZ-Fa-BZ.

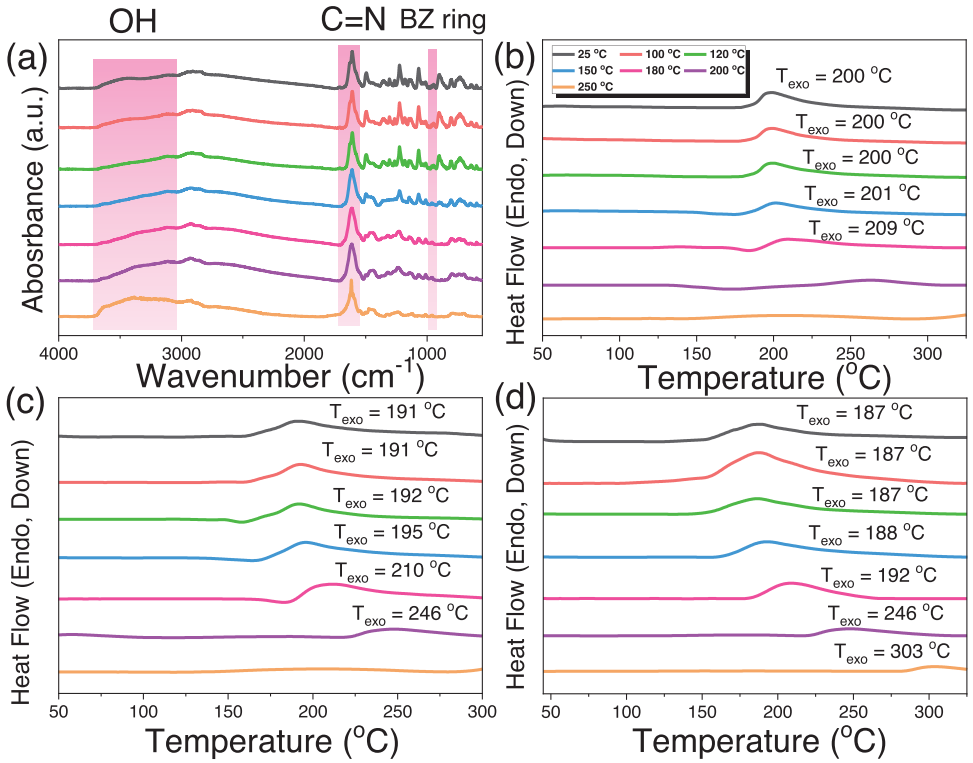

Figure 8. a) FTIR analyses of BAZ-Th-BZ/BAZ-Fa-BZ and DSC profiles of BAZ-Th-BZ/BAZ-Fa-BZ = b) 3/1, c) 1/1, and d) 1/3.

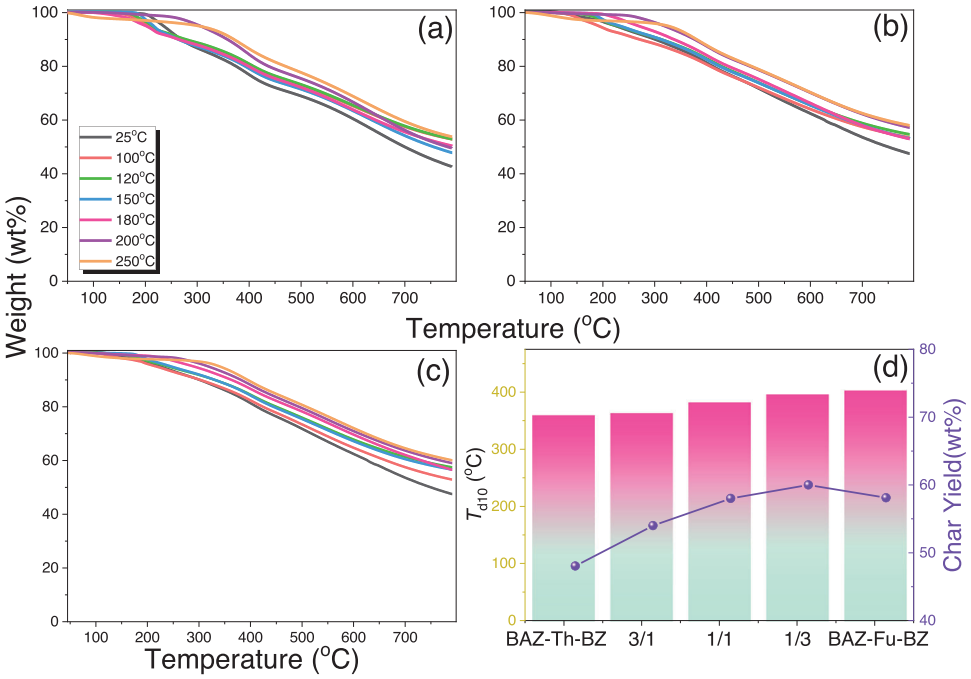

Figure 9. TGA analyses of BAZ-Th-BZ/BAZ-Fa-BZ after thermal treatment: a) 3/1, b) 1/1, c) 1/3, and d) T_{d10} values and char yields of BAZ-Th-BZ/BAZ-Fa-BZ at 250 °C.

BZ ring in the BAZ-Th-BZ/BAZ-Fa-BZ undergoes the ROP reaction, as observed in Figure 9a–c, leading to increased formation of hydrogen bonds from the ring opening of the BZ group and between the azine units, and formation crosslinked network structure; thereby enhancing the thermal stability of the blends. With an increase in the BAZ-Fa-BZ ratio, the proportion of the Th group decreases, increasing the char yield. Figure 9d clearly demonstrates a rise in the char yield of BAZ-Th-BZ/BAZ-Fa-BZ corresponding to the BAZ-Fa-BZ content. This alignment with expectations is attributed to the anticipated reduced char yield due to the influence of the Th group from BAZ-Th-BZ.

2.4. Photoluminescence Property of BAZ-Th-BZ/BAZ-Fa-BZ

The UV–vis absorption analyses conducted on BAZ-Fa-BZ and BAZ-Th-BZ monomers dissolved in tetrahydrofuran (THF) at a 10^{-6} M concentration revealed a distinct absorption peak around 370 nm. This observation suggested that the π–π^* transition was influenced by the presence of the salicylaldazine, furan, and Th units, as depicted in **Figure 10a**. Most of the salicylaldehyde azines that have been studied glow when they are clumped together. This is probably because of RIR and excited-state intramolecular proton transfer (ESIPT) characters.[64] In solid-state photoluminescence (PL) analyses, emission bands were observed at 535, 542, 553, 549, and 546 nm for BAZ-Th-BZ, BAZ-Th-BZ/BAZ-Fa-BZ blends with ratios ranging from 3/1 to 1/1, and BAZ-Fa-BZ, respectively (Figure 10b). The robust emissions at 535 nm for pure BAZ-Th-BZ and 546 nm for pure BAZ-Fa-BZ resulted from intramolecular hydrogen bonding within the salicylaldazine units, coupled with the ESIPT character. Moreover, the emission intensities of their BAZ-Th-BZ/BAZ-Fa-BZ blends were diminished compared to the BAZ-Th-BZ and BAZ-Fa-BZ monomers.

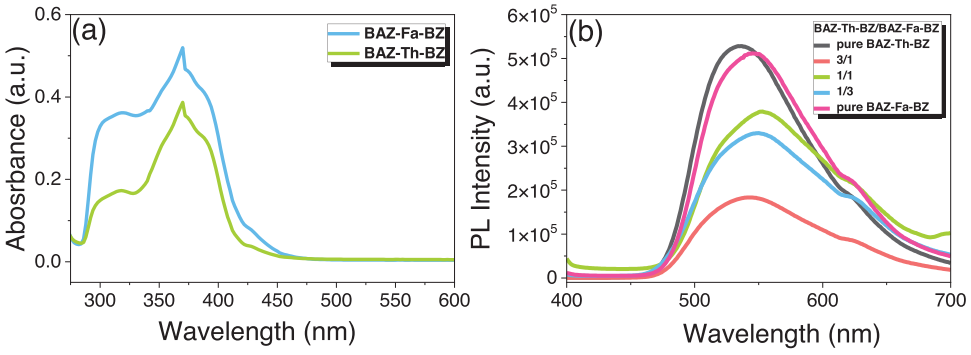

Figure 10. a) UV–vis absorption analyses of BAZ-Fa-BZ and BAZ-Th-BZ. b) PL analyses of the solid state of BAZ-Th-BZ/BAZ-Fa-BZ.

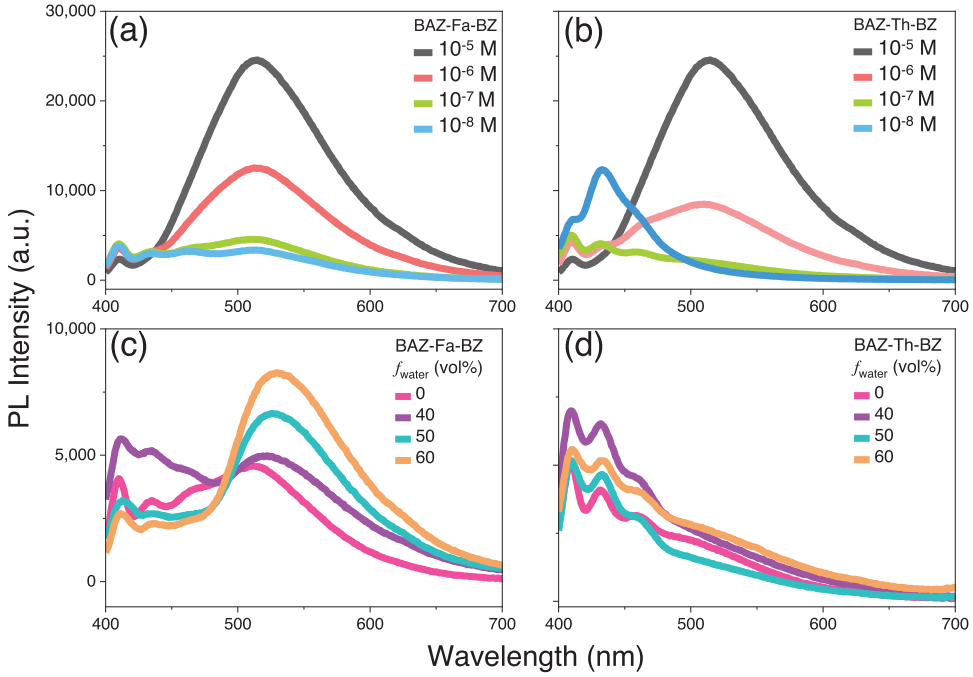

Figure 11. PL spectra of various concentrations of a) BAZ-Fa-BZ and b) BAZ-Th-BZ in THF solution. PL profiles of c) BAZ-Fa-BZ and d) BAZ-Th-BZ in THF/H_2O with an excitation wavelength of 365 nm.

In **Figure 11**a,b, it is noteworthy that BAZ-Fa-BZ and BAZ-Th-BZ were prepared at different concentrations in THF. When the concentration of BAZ-Fa-BZ and BAZ-Th-BZ increased from 10^{-8} to 10^{-5} M, the fluorescence intensities increased, indicating AIE behavior of BAZ-Fa-BZ and BAZ-Th-BZ due to ESIPT and restricted intramolecular rotation character (RIR).[65–70] We investigated the AIE phenomena of BAZ-Fa-BZ and BAZ-Th-BZ in THF/H_2O co-solvent ranging from 0% to 60%. Both BAZ-Fa-BZ and BAZ-Th-BZ could dissolve in THF but were insoluble in water. As illustrated in Figure 11c,d, the fluorescence intensity of BAZ-Fa-BZ reached its highest peak at a water fraction (f_{water}) of 60%. In contrast, for BAZ-Th-BZ, the fluorescence intensity showed an increase in f_{water} of both 40% and 60%. The emissions' behavior observed in THF/H_2O mixtures from BAZ-Fa-BZ and BAZ-Th-BZ likely resulted from aggregate formation, suggesting the presence of AIE in both BAZ-Fa-BZ and BAZ-Th-BZ.

3. Conclusions

In this study, we employed the Mannich condensation method to develop a novel salicylaldazine bisbenzoxazine resin incorporating Fa and Th units. The successful synthesis of bisbenzoxazine monomers enriched with furan and thiophene was confirmed through FTIR and NMR analyses, which provided molecular characterizations of the synthesized compounds. Moreover, the ROP of BAZ-Fa-BZ and BAZ-Th-BZ, along with the thermal properties of the resulting PBZ, was thoroughly investigated through DSC, FTIR, and TGA analyses. Based on the DSC data, we observed that the exothermic curing peak of BAZ-Fa-BZ occurred at a lower temperature (197 °C) compared to that of BAZ-Th-BZ (214 °C). Poly(BAZ-Fa-BZ) exhibited superior thermal properties compared to poly(BAZ-Th-BZ), featuring a T_{d10} of 402 °C, a char yield of 58 wt% after thermal curing treatment at 250 °C, and a decreased surface free energy of 28.9 mJ m^{-2}. In addition, the poly(BAZ-Th-BZ/BAZ-Fa-BZ) blend with a higher content of BAZ-Fa-BZ after thermal treatment at 250 °C exhibited the highest char yield at 60 wt% and a T_{d10} of 395 °C. Furthermore, the identification of bisbenzoxazines abundant in furan and thiophene moieties opens up numerous possibilities for advancing high-performance PBZ thermosets with auspicious applications.

4. Experimental Section

Materials: 1,4-Dioxane (1,4-DO, purity = 98%) and $(CH_2O)_n$ were obtained from Sigma–Aldrich. Fa—NH_2 (purity = 97%), Th—NH_2 (purity = 98%), ethyl acetate (EAc, purity = 99%), and THF (purity = 99%) were purchased from Alfa-Aesar. BAZ—4OH was prepared following the previously published procedure (Figures S1–S3, Supporting Information).[65]

Synthesis of BAZ-Fa-BZ: In a 100 mL flask, under a nitrogen atmosphere equipped with a reflux condenser, a mixture of $(CH_2O)_n$ (0.44 g, 14.6 mmol), BAZ—4OH (1.00 g, 3.67 mmol), and Fa—NH_2 (0.78 mL, 7.31 mmol) in 50 mL of 1,4-DO was prepared. The mixture was refluxed at 100 °C for the entire day. Subsequently, the solution was concentrated using a rotary evaporator to yield a rust-colored solid. This solid was further purified through column chromatography (SiO_2: EAc as an eluent) to obtain a mustard-colored solid (1.76 g, yield: 93%). The purity of BAZ-Fa-BZ and BAZ-Th-BZ reached up to 99%.

Synthesis of BAZ-Th-BZ: Under a nitrogen atmosphere, $(CH_2O)_n$ (0.44 g, 14.6 mmol), BAZ—4OH (1.00 g, 3.67 mmol), and Th—NH_2 (0.75 mL, 7.34 mmol) were combined with 50 mL of 1,4-DO in a 100 mL flask equipped with a reflux condenser. The mixture underwent reflux at 100 °C for a full day. Following this, the solution was subjected to rotary evaporation, yielding a solid with a rust-colored appearance. Subsequent purification via column chromatography (SiO_2: EAc), resulted in the

isolation of a yellow solid (1.80 g, yield: 90%). The purity of BAZ-Th-BZ reached up to 98%.

Preparation of Poly(BAZ-Fa-BZ) and Poly(BAZ-Th-BZ): During the thermal treatment, varying weights of BAZ-Fa-BZ or BAZ-Th-BZ were subjected to temperatures ranging from 100 to 250 °C for 2 h. Consequently, each poly(BAZ-Fa-BZ) or poly(BAZ-Th-BZ) transitioned in color from orange to black solid.

Preparation of BAZ-Th-BZ/BAZ-Fa-BZ Blends and Poly(BAZ-Th-BZ/BAZ-Fa-BZ): The different weight ratios of BAZ-Th-BZ/BAZ-Fa-BZ were combined in THF and allowed to mix for 1 day. Subsequently, the solution was evaporated using a rotary evaporator to obtain the BAZ-Th-BZ/BAZ-Fa-BZ materials. Later on, the resulting blends underwent thermal treatment for 2 h at temperatures ranging from 100 to 250 °C. As a result, each poly(BAZ-Th-BZ/BAZ-Fa-BZ) changed in color from orange to black.

Supporting Information

Supporting Information is available from the Wiley Online Library or from the author.

Acknowledgements

This study was supported financially by the National Science and Technology Council, Taiwan, under contracts NSTC 112-2221-E-110 –003.

Conflict of Interest

The authors declare no conflict of interest.

Data Availability Statement

Research data are not shared.

Keywords

benzoxazine, emission properties, ring-opening polymerization, surface free energy, thermal properties

Received: March 28, 2024
Revised: May 19, 2024
Published online: June 7, 2024

[1] Y. Lu, Y. Zhang, K. Zhang, *Chem. Eng.* **2022**, *448*, 137670.
[2] H. Lin, X. Lu, A. Lu, M. Yuan, Z. Xin, *J. Polym. Sci.* **2023**, *61*, 2333.
[3] Y. Lu, J. Liu, W. Zhao, K. Zhang, *Chem. Eng. J.* **2023**, *457*, 141232.
[4] X. Fan, Z. Liu, J. Huang, D. Han, Z. Qiao, H. Liu, J. Du, H. Yan, Y. Ma, C. Zhang, Z. Wang, *Adv. Compos. Hybrid Mater.* **2022**, *5*, 322.
[5] Y. C. Kao, W. C. Chen, A. F. M. EL-Mahdy, M. G. Mohamed, M. Ejaz, S. W. Kuo, *Macromol. Chem. Phys.* **2023**, *224*, 2300153.
[6] X. Kang, Z. Lu, W. Feng, X. Fang, J. Wang, X. Fang, Y. Xu, Y. Wang, B. Liu, T. Ding, Y. Ma, D. Pan, R. P. Patil, V. Murugadoss, *Adv. Compos. Hybrid Mater.* **2021**, *4*, 127.
[7] C. Y. Chen, W. C. Chen, M. G. Mohamed, Z. Y. Chen, S. W. Kuo, *Macromol. Rapid Commun.* **2023**, *44*, 2200910.
[8] Y. Xing, Y. Zhang, X. He, *Polym. Bull.* **2023**, *80*, 12065.
[9] I. Machado, I. Hsieh, E. Rachita, M. L. Salum, D. Iguchi, N. Pogharian, A. Pellot, P. Froimowicz, V. Calado, H. Ishida, *Green Chem.* **2021**, *23*, 4051.
[10] M. Yang, T. Wang, Y. Tian, H. Zhang, J. Zhang, J. Cheng, *Green Chem.* **2024**, *26*, 4771.
[11] K. D. Demir, B. Kiskan, S. S. Latthe, A. L. Demirel, Y. Yagci, *Polym. Chem.* **2013**, *4*, 2106.
[12] L. Jin, T. Agag, H. Ishida, *Eur. Polym. J.* **2010**, *46*, 354.
[13] M. G. Mohamed, S. W. Kuo, *Macromol. Chem. Phys.* **2019**, *220*, 1800306.
[14] S. Gulyuz, Y. Yagci, B. Kiskan, *Polym. Chem.* **2022**, *13*, 3631.
[15] P. Mora, S. Rimdusit, P. Karagiannidis, U. Srisorrachatr, C. Jubsilp, *BIOB* **2023**, *10*, 62.
[16] S. Gulyuz, Y. Yagci, B. Kiskan, *Macromolecules* **2024**, *57*, 2078.
[17] M. G. Mohamed, S. W. Kuo, A. Mahdy, I. M. Ghayd, K. I. Aly, *Mater. Today Commun.* **2020**, *25*, 101418.
[18] X. Zhou, F. Fu, M. Shen, Q. Li, H. Liu, Z. Song, *Adv. Sustainable Syst.* **2024**, *8*, 2300372.
[19] M. G. Mohamed, C. C. Chen, K. Zhang, S. W. Kuo, *Eur. Polym. J.* **2023**, *200*, 112551.
[20] N. Muthukumar, H. Arumugam, B. Krishnasamy, M. Athianna, A. Muthukaruppan, *ChemistrySelect* **2023**, *8*, 202204302.
[21] X. L. Sha, P. Fei, B. Shen, J. Chen, Z. Liu, Y. Sun, J. T. Miao, *ACS Appl. Polym. Mater.* **2023**, *5*, 3015.
[22] Y. C. Kao, J. Y. Lin, W. C. Chen, M. G. Mohamed, C. F. Huang, J. H. Chen, S. W. Kuo, *Polymers* **2024**, *16*, 112.
[23] X. Zhang, M. G. Mohamed, Z. Xin, S. W. Kuo, *Polymer* **2020**, *201*, 122552.
[24] C. F. Wang, Y. C. Su, S. W. Kuo, C. F. Huang, Y. C. Sheen, F. C. Chang, *Angew. Chem., Int. Ed.* **2006**, *45*, 2248.
[25] J. Liu, X. Lu, Z. Xin, C. Zhou, *Langmuir* **2013**, *29*, 411.
[26] C. H. Chiang, M. G. Mohamed, W. C. Chen, M. Madhu, W. L. Tseng, S. W. Kuo, *Polymers* **2023**, *15*, 331.
[27] H. Jia, N. Xu, Y. Nagai, M. Doi, T. Sawada, T. Serizawa, S. Ando, S. Habuchi, T. Michinobu, *Polym. Chem.* **2023**, *14*, 2510.
[28] J. Xu, J. Wang, O. M. Bakr, N. Hadjichristidis, *Angew. Chem.* **2023**, *135*, 202217418.
[29] H. Yan, Y. He, D. Wang, T. Han, B. Z. Tang, *Aggregate* **2023**, *4*, 331.
[30] J. H. Xin, B. B. Guo, C. Liu, C. Y. Zhu, H. Zhang, B. Z. Tang, Z. K. Xu, *Macromolecules* **2023**, *56*, 5415.
[31] M. G. Mohamed, H. Y. Hu, M. Madhu, M. M. Samy, I. M. A. Mekhemer, W. L. Tseng, H. H. Chou, S. W. Kuo, *Eur. Polym. J.* **2023**, *189*, 111980.
[32] S. Yu, K. Liu, Y. Tian, X. Chen, J. Zhang, M. Gao, J. Wang, M. Zhang, C. Zhao, *Macromolecules* **2023**, *56*, 4278.
[33] L. Lu, K. Wang, H. Wu, A. Qin, B. Z. Tang, *Chem. Sci.* **2021**, *12*, 7058.
[34] P. Q. Nhien, H. K. Chang, T. T. K. Cuc, T. M. Khang, C. H. Wu, B. T. B. Hue, J. I. Wu, H. C. Lin, *Sens. Actuators, B* **2022**, *372*, 132634.
[35] R. Hu, A. Qin, B. Z. Tang, *Prog. Polym. Sci.* **2020**, *100*, 101176.
[36] Y. Qian, M. M. Cai, X. H. Zhou, Z. Q. Gao, X. P. Wang, Y. Z. Zhao, X. H. Yan, W. Wei, L. H. Xie, W. Huang, *J. Phys. Chem. C* **2012**, *116*, 12187.
[37] Z. Q. Xie, B. Yang, G. Cheng, L. L. Liu, F. He, F. Z. Shen, Y. G. Ma, S. Y. Liu, *Chem. Mater.* **2005**, *17*, 1287.
[38] Z. P. Yu, Y. Y. Duan, L. H. Cheng, Z. L. Han, Z. Zheng, H. P. Zhou, J. Y. Wu, Y. P. Tian, *J. Mater. Chem.* **2012**, *22*, 16927.
[39] H. A. Molla, R. Bhowmick, A. Katarkar, K. Chaudhuri, S. Gangopadhyay, M. Ali, *Anal. Methods* **2015**, *7*, 5149.
[40] H. C. Liu, W. C. Su, Y. L. Liu, *J. Mater. Chem.* **2011**, *21*, 7182.
[41] Y. Su, W. Shi, X. Chen, S. Zhao, Y. Hui, Z. Xie, *RSC Adv.* **2016**, *6*, 41340.
[42] W. Shi, Q. Liu, J. Zhang, X. Zhou, C. Yang, K. Zhang, Z. Xie, *Polym. Chem.* **2019**, *10*, 1130.
[43] F. Li, W. Zhang, J. Wang, *Eur. Polym. J.* **2023**, *199*, 112466.
[44] Y. Lu, N. Li, Y. Peng, M. G. Mohamed, S. W. Kuo, K. Zhang, *Mol. Syst. Des. Eng.* **2024**, *9*, 86.
[45] S. Mukherjee, B. Lochab, *Macromolecules* **2024**, *57*, 1795.
[46] R. Yang, M. Han, B. Hao, K. Zhang, *Eur. Polym. J.* **2020**, *131*, 109706.

[47] M. G. Mohamed, C. J. Li, M. A. R. Khan, C. C. Liaw, K. Zhang, S. W. Kuo, *Macromolecules* **2022**, *55*, 3106.
[48] S. M. Zhang, J. Q. Zhao, Y. Liu, Y. X. Liu, C. M. Liu, *React. Funct. Polym.* **2021**, *165*, 104957.
[49] H. Ding, X. Wang, L. Song, Y. Hu, *J. Renewable Mater.* **2022**, *10*, 871.
[50] S. Mukherjee, B. Lochab, *Chem. Commun.* **2022**, *58*, 3609.
[51] N. Li, S. Yang, K. Zhang, *Macromolecules* **2023**, *56*, 6667.
[52] Y. Lyu, L. Qiu, *Polym. Degrad. Stab.* **2022**, *196*, 109829.
[53] Y. Lyu, Y. Zhang, H. Ishida, *Eur. Polym. J.* **2020**, *133*, 109770.
[54] M. M. Samy, M. G. Mohamed, S. W. Kuo, *Eur. Polym. J.* **2020**, *138*, 109954.
[55] Z. Wang, L. Qi, Z. Yuan, A. A. K. Gorar, A. Q. Day, W. B. Liu, J. Wang, J. Y. Wang, *React. Funct. Polym.* **2024**, *194*, 105802.
[56] Y. Liu, C. I. Chou, *J. Polym. Sci., Part A: Polym. Chem.* **2005**, *43*, 5267.
[57] C. Wang, J. Sun, X. Liu, A. Sudo, T. Endo, *Green Chem.* **2012**, *14*, 2799.
[58] X. Shen, L. Cao, Y. Liu, J. Dai, X. Liu, J. Zhu, S. Du, *Macromolecules* **2018**, *51*, 4782.
[59] H. D. Kim, H. Ishida, *J. Phys. Chem. A* **2002**, *106*, 3271.
[60] M. Kazim, L. Guan, A. Chopra, R. Sun, M. A. Siegler, T. Lectka, *J. Org. Chem.* **2020**, *85*, 9801.
[61] S. Nakamura, Y. Tsuji, K. Yoshizawa, *ACS Omega* **2020**, *5*, 26211.
[62] P. Mills, S. Korlann, M. E. Bussell, M. A. Reynolds, M. V. Ovchinnikov, R. J. Angelici, C. Stinner, T. Weber, R. Prins, *J. Phys. Chem. A* **2001**, *105*, 4418.
[63] Z. Yao, Y. Lu, J. Song, K. Zhang, *Molecules* **2023**, *28*, 5077.
[64] W. Tang, Y. Xiang, A. Tong, *J. Org. Chem.* **2009**, *74*, 2163.
[65] M. G. Mohamed, R. C. Lin, J. H. Tu, F. H. Lu, J. L. Hong, K. U. Jeong, C. F. Wang, S. W. Kuo, *RSC Adv.* **2015**, *5*, 65635.
[66] L. C. Chou, M. G. Mohamed, S. W. Kuo, Y. Nakamura, C. F. Huang, *Chem. Commun.* **2022**, *58*, 12317.
[67] M. Ahmed, A. F. M. EL-Mahdy, *Macromolecules* **2024**.
[68] M. G. Mohamed, F. H. Lu, J. L. Hong, S. W. Kuo, *Polym. Chem.* **2015**, *6*, 6340.
[69] X. Zhang, H. Liu, G. Zhuang, S. Yang, P. Du, *Nat. Commun.* **2022**, *13*, 3543.
[70] Y. Song, J. Dong, J. Yuan, X. Zhang, G. Wu, E. Zhang, G. Feng, L. Wu, S. Lei, W. Hu, *J. Mater. Chem. C* **2023**, *11*, 10230.